



Image quality analysis and comparison of three radar-based breast microwave sensing systems

Tyson Reimer¹ , Gabrielle Fontaine¹ , Fatimah Eashour¹, Jordan Krenkevich¹ and Stephen Pistorius^{1,2}

¹Department of Physics and Astronomy, University of Manitoba, Winnipeg, Manitoba, Canada and ²CancerCare Manitoba Foundation, Winnipeg, Manitoba, Canada

Research Paper

Cite this article: Reimer T, Fontaine G, Eashour F, Krenkevich J, Pistorius S (2025) Image quality analysis and comparison of three radar-based breast microwave sensing systems. *International Journal of Microwave and Wireless Technologies*, 1–10. <https://doi.org/10.1017/S1759078725000376>

Received: 29 September 2024
Revised: 12 February 2025
Accepted: 8 March 2025

Keywords:

breast cancer; image quality; microwave imaging; radar

Corresponding author: Gabrielle Fontaine;
Email: fontai26@myumanitoba.ca

Abstract

Several breast microwave sensing (BMS) systems have shown encouraging results as a potential breast cancer detection tool. The existing systems in the literature have diverse designs, equipment, measurement protocols, and analysis methods. However, there is relatively little investigation on the impact and performance of varying system designs. This work compares the impact of system design parameters on three existing BMS systems. The first system, a bed-based system, was designed for use in a permanent clinic. The second system, a bench-top system, was created for laboratory research. The third system, a portable system, was designed for use in low-income and remote communities. The bed-based system had the highest resolving capabilities, achieving a spatial resolution of 12.4 ± 0.5 mm. Additionally, the bed system had the highest signal-to-noise ratio of 26 ± 1 dB. The portable system had the least intensity dependence on polar positions within the imaging chamber. The bed system had the highest contrast between tumor- and adipose-mimicking materials. However, the contrast of tumor- and fibroglandular-mimicking materials was similar for each system. By comparing and evaluating the performance of multiple BMS systems, we improve our understanding of system design, allowing for potential studies into an ideal BMS system.

Introduction

Breast cancer is one of the most prevalent cancers, affecting millions of women annually [1], and early detection plays a crucial role in improving survival rates [1–3]. Traditional breast cancer detection methods, such as X-ray mammography, magnetic resonance imaging (MRI), and ultrasound, are well-established but have several limitations, particularly with regard to their application in resource-limited, low and middle-income countries, and other marginalized communities [4–6]. These methods are often costly, large, use fragile equipment, require good infrastructure, and require trained personnel to operate and interpret images [2, 7].

Given these challenges, there is an increasing need for alternative screening methods that are cost-effective, safe, and portable. Breast microwave sensing (BMS) has emerged as a promising approach for breast cancer detection due to its non-ionizing nature, smaller size, lower cost, and potential for use in diverse clinical environments [7, 8]. Unlike traditional methods, BMS operates by exploiting the dielectric contrast between malignant and healthy breast tissues, making it an attractive candidate for early detection in both developed and developing regions.

In recent years, research into BMS has led to the development of various systems, each with differing designs, equipment configurations, measurement protocols, and analysis techniques [8–10]. As a result, the performance of BMS systems can vary significantly. Factors such as antenna design, frequency range, and signal and image processing algorithms directly impact the accuracy and diagnostic capabilities of each system. Despite the advances, there remains a lack of comprehensive studies comparing image quality and diagnostic metrics across different BMS platforms.

Current BMS systems have primarily been evaluated through numerical simulations, physical breast phantoms, and, in some cases, early-stage clinical trials. However, the reported diagnostic specificity ranges from 20% to 65% [11, 12], suggesting that the system design plays a critical role in diagnostic success. Despite this, little attention has been given to traditional image quality metrics such as spatial resolution, contrast resolution, noise, and artifacts—parameters that are crucial for both characterizing and optimizing BMS systems before progressing to clinical applications.

In this work, we expand on the evaluation and comparison of three distinct BMS systems in [13]. These systems include a (a) bed-based system designed for long-term clinical use, (b)

© The Author(s), 2025. Published by Cambridge University Press in association with The European Microwave Association. This is an Open Access article, distributed under the terms of the Creative Commons Attribution licence (<http://creativecommons.org/licenses/by/4.0>), which permits unrestricted re-use, distribution and reproduction, provided the original article is properly cited.

bench-top model for laboratory research, and (c) portable system targeted at low-income and remote areas. These systems differ in several critical aspects, including frequency bandwidth, angular sampling, antenna configuration, and the analysis used.

To ensure rigorous comparison, we employed 3D-printed phantoms to assess spatial resolution, signal-to-noise, image accuracy, and contrast resolution. By providing a comprehensive characterization of each system, this work aims to inform the future development of more efficient and accurate BMS designs, ultimately contributing to the enhancement of breast cancer screening technologies.

Methods

Microwave sensing systems

In this study, three BMS systems were evaluated using several image quality analysis tools. These systems include a bed-based system, bench-top system, and portable system, each designed for different applications (Fig. 1). Their designs and measurement parameters are summarized in Table 1. Each system operates in the air to minimize system complexity.

- (1) **The Bed-Based System:** This system [14] employs a bistatic design with two horn antennas mounted on a rotating platform. A Copper Mountain (C1209, Copper Mountain Technologies, IN, USA) vector network analyzer (VNA), which rotates with the antennas, was used to capture 2-port scattering parameters across 1001 frequency points in the 2.0–9.0 GHz range. Designed for clinical settings, this system uses a bed to provide patient comfort during scanning.
- (2) **The Bench-top System:** Created for laboratory research, this system comprises 24 Vivaldi antennas arranged along a 20 cm diameter cylindrical path. Scans are performed using a 2-port VNA (Planar 804/1, Copper Mountain Technologies, IN, USA) connected to an electromechanical 2×24 switch matrix, covering a frequency range of 0.7–8.0 GHz with 1001 frequency points. While capable of 24×24 S-parameter measurements, only S_{11} data were utilized in this study for image reconstruction.
- (3) **The Portable System:** Designed for low-resource settings, this system [15] integrates 24 ultra-wideband (UWB) antennas in a 20 cm diameter cylindrical array. Each antenna is connected to an inexpensive NanoVNA V2-Plus device, allowing for the collection of S_{11} data between 0.7 and 4.4 GHz at 381 frequency points. The system prioritizes portability and cost-effectiveness through compact, affordable components and a simplified geometric configuration, making it suitable for use in remote or low-income communities.

For this work, the standard delay-and-sum (DAS) beamformer was used to reconstruct images with all three systems.

Evaluation of spatial resolution

Spatial resolution, a critical metric for image quality, was assessed using three methods:

- (1) **Time-Domain (TD) Full-Width Half-Max (FWHM) Analysis:** Scans were performed with a single rod at various positions within the system using the positioning system in Fig. 2a. The frequency domain S_{11} measurements were

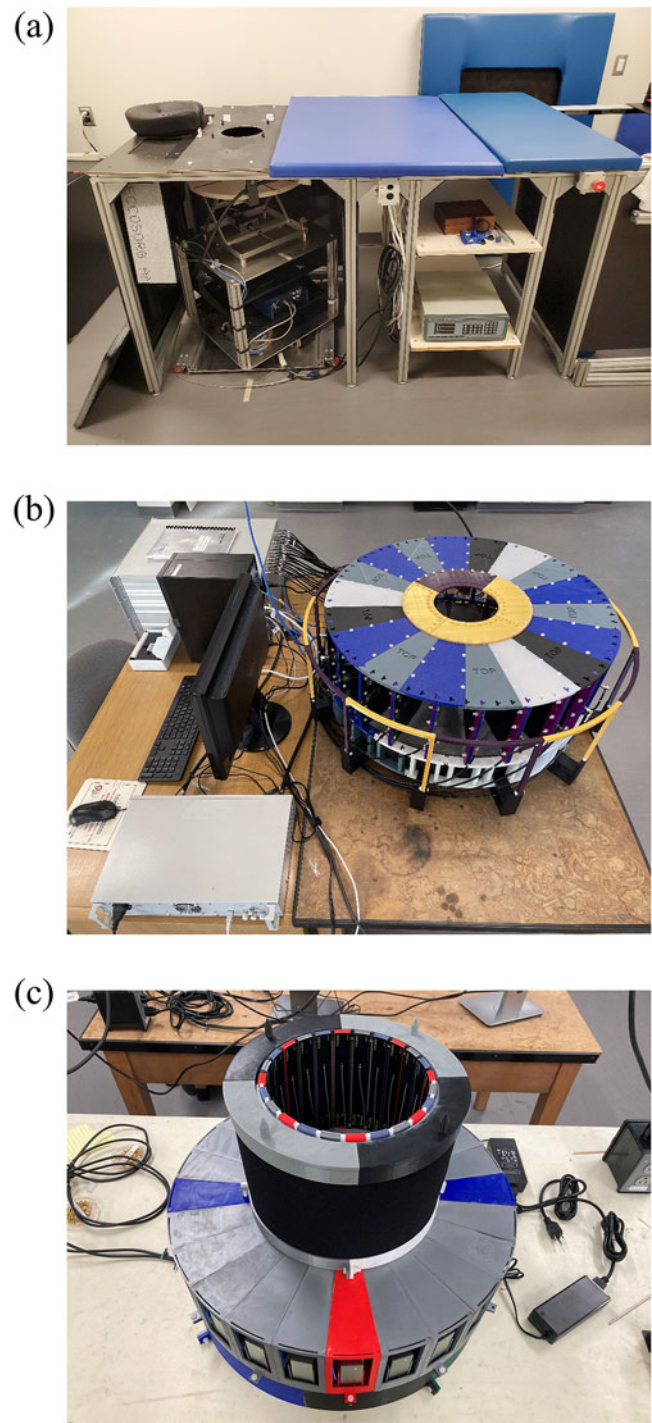


Figure 1. The three BMS used in this work: (a) Bed-based imaging system, (b) Bench-top system, and (c) Portable system.

converted to the time domain using the inverse chirp z-transform [16]. From here, the spatial resolution was defined as $d = \text{FWHM}_t \times c/2$, where c is the speed of light in air and FWHM_t is the full-width half-maximum of the rod's time-domain S_{11} signal.

- (2) **Modulation Transfer Function (MTF) Analysis:** DAS-reconstructed images of the single-rod scans were analyzed using the method in [17]. The point-spread function (PSF)

Table 1. Parameters of the three BMS systems used in this work

	Bed System	Intermediate System	Portable System
Frequency Range	2.0–9.0 GHz	0.7–8.0 GHz	0.6–4.4 GHz
Bandwidth	7.0 GHz	7.3 GHz	3.8 GHz
Fractional Bandwidth	1.27	1.68	1.52
Number of Frequencies	1001	1001	381
IF Bandwidth	10 kHz	10 kHz	10 kHz
Output Power	15 dBm	10 dBm	-13 dBm
Multistatic Array	✗	✓	✓
Mechanical Motion	✓	✗	✗
Number of Antennas	2	24	24
Antenna Type	Horn	Vivaldi	UWB
Number of Angular Positions	72	24	24
VNA	C1209 (Copper Mountain)	Planar 804/1 (Copper Mountain)	NanoVNA V2-Plus

was determined, which characterizes the system’s response to a point source. The PSF was converted to its MTF to calculate the spatial resolution, representing the best-case scenario in the absence of scattering.

- (3) **Two-Target Analysis:** Using a dual-rod positioning system illustrated in Fig. 2b, scans were conducted with rods placed at varying separation distances. Images were created using the DAS reconstruction method. Similar to the method in [17], the MTF was used to analyze the intensity responses along the 1D cross-section intersecting the two-rod responses. Spatial resolution was defined as the minimum distance at which the two targets became distinguishable, which was defined as the intensity between the two rods being less than 90% of the smaller maximum intensity.

Evaluation of data and image noise

Noise levels were evaluated using a 3D-printed cylindrical phantom filled with a solution of 5% water and 95% diethylene glycol monobutyl ether (DGBE), mimicking the dielectric properties of adipose tissue (Fig. 3).

The noise in the data was quantified by calculating the mean and standard deviation of differences between repeated S_{11} measurements. The data signal-to-noise ratio (SNR), defined as the mean and standard deviation of the differences between repeated scans, was computed to assess data quality. Image noise was evaluated by analyzing differences in reconstructed images from repeated scans of the phantom. The image SNR was defined as,

$$SNR = \frac{1}{V} \sum_{\mathbf{r} \in V} \frac{I(\mathbf{r})^{(n)}}{|I(\mathbf{r})^{(n)} - I(\mathbf{r})^{(n+1)}|} \tag{1}$$

where $I(\mathbf{r})^{(n)}$ is the n^{th} image and V is the volume of the imaging domain.

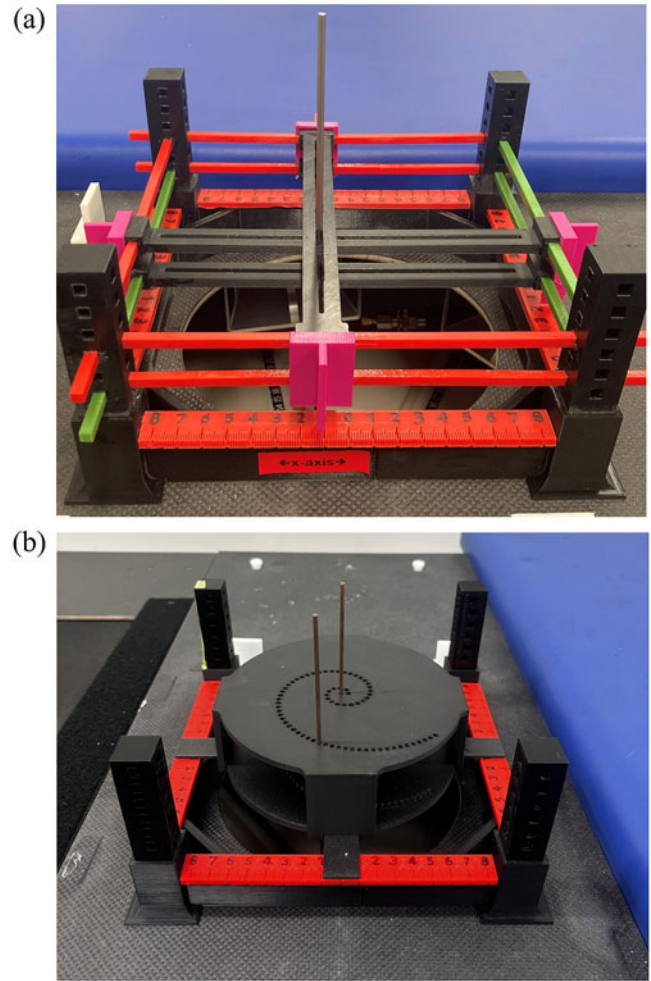


Figure 2. (a) Single-rod positioning system, and (b) dual-rod positioning system used to evaluate spatial resolution.



Figure 3. 3D-printed cylindrical phantom used to evaluate noise.

Evaluation of image accuracy

The accuracy of reconstructed images was assessed by scanning a single rod placed at different locations within the imaging chamber. Given the inherent non-linearity in microwave imaging due

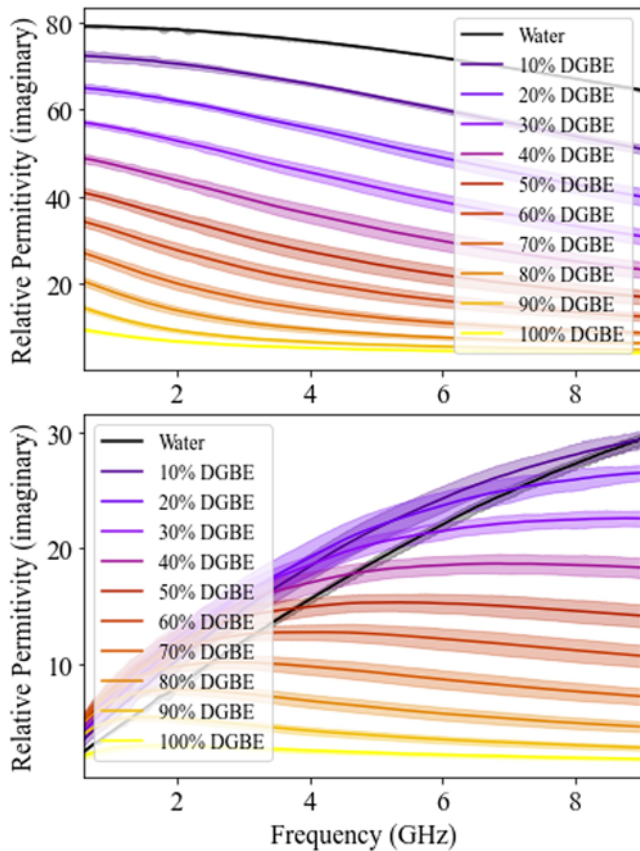


Figure 4. The real (top) and imaginary (bottom) relative permittivity of varying DGBE–water liquid solutions from 0.6 to 9 GHz.

to factors such as antenna characteristics, the ideal response of a point-like object should be symmetric and independent of its position. To assess this, the maximum image intensity I_{max} of the rod was measured at varying polar distances from the center of the imaging chamber, allowing for the detection of position-dependent intensity.

Evaluation of contrast

Contrast resolution, an essential metric for differentiating tissues with similar dielectric properties, was evaluated using 3D-printed cylinders (Fig. 5) filled with varying concentrations of DGBE and de-ionized water. Eleven liquid samples were prepared, with relative permittivities measured using an open-ended coaxial probe (DAK 3.5, SPEAG, Zurich, Switzerland) from 0.6 to 9 GHz (Fig. 4). These samples mimicked the dielectric properties of adipose, fibroglandular, and tumor tissues.

For each scan, one cylinder was filled with water (representing tumor tissue), while the other contained one of the DGBE–water mixtures (representing different types of breast tissues). The DAS reconstruction method was applied to produce images of the cylinders, and the contrast was quantified using intensity-volume histograms (IVHs). The IVHs assess the percent-volume of the target that has an intensity greater than I , where I is varied between zero and the maximum target intensity. These IVHs plot the percent volume of a target versus image intensity, providing a quantitative measure of contrast between different tissue types.

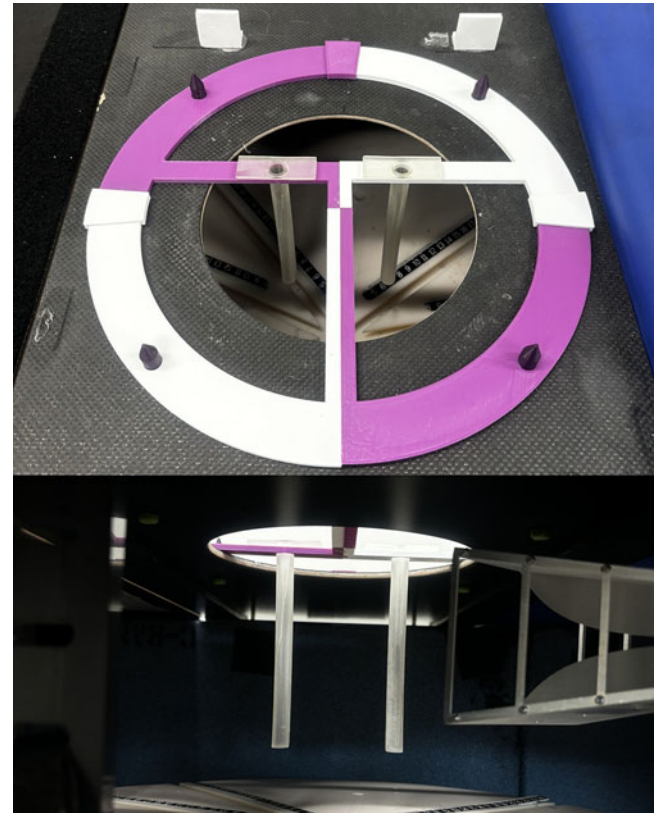


Figure 5. 3D-printed cylinders that were filled with varying solutions of DGBE and water to examine the contrast capabilities of the imaging systems.

Table 2. Spatial resolution of the microwave imaging systems

	Spatial resolution (mm)		
	TD-FWHM	MTF-based	Two-target
Bed system	29.5 ± 0.7	12.4 ± 0.5	18 ± 1
Bench-top system	36 ± 3	18 ± 1	26 ± 1
Portable system	57 ± 8	24.5 ± 0.9	46 ± 1

The contrast between two targets can be defined between the horizontal spacing of two IVH curves,

$$C_v^{\%} = \frac{I_{\text{left}} - I_{\text{right}}}{\frac{1}{2}(I_{\text{left}} + I_{\text{right}})} \quad (2)$$

where $C_v^{\%}$ is the contrast at a given percent-volume, I_{left} is the intensity of the left cylinder, and I_{right} is the intensity of the right cylinder.

Results

Spatial resolution

The spatial resolution results for the three BMS systems are summarized in Table 2. Overall, the bed-based system achieved the highest spatial resolution across all evaluation methods. Using the MTF-based method, the bed-based system demonstrated a spatial resolution of 12.4 mm ± 0.5 mm.

The two-target analysis (Fig. 6) yielded slightly lower resolution values due to the inclusion of scattering between the rods, which

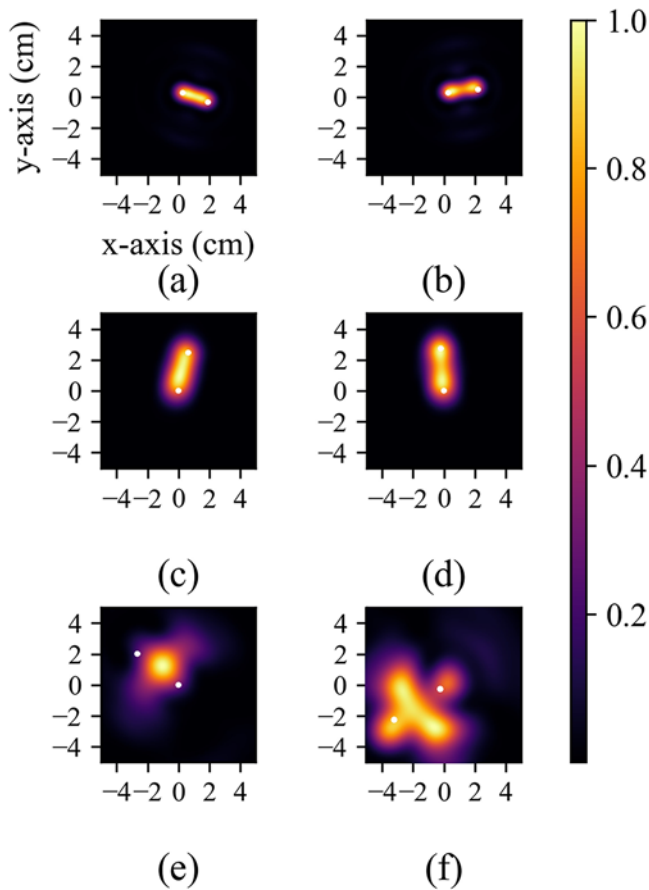


Figure 6. Two-target image analysis displaying indistinguishable (left) and distinguishable (right) targets of the bed system (a, b), bench-top system (c, d), and portable system (e, f).

more accurately reflects the conditions encountered in complex imaging environments.

Table 3. Data and image noise of the microwave imaging systems

	Data SNR _D (dB)	Image SNR (dB)
Bed system	26 ± 1	26 ± 2
Bench-top system	22 ± 2	14 ± 4
Portable system	7.9 ± 0.6	13 ± 3

The time-domain FWHM method exhibited the poorest spatial resolution for all systems, with the bed-based system providing a resolution of 29.5 ± 0.7 mm.

Noise

The noise levels in the three systems were assessed through both data and image noise analysis. Table 3 presents the signal-to-noise ratio (SNR) results for both methods. The bed-based system exhibited the highest data and image SNRs, with values of 26 ± 1 and 26 ± 2 dB, respectively.

The bench-top system had a data SNR of 22 ± 2 dB but a much lower image SNR of 14 ± 4 dB. This discrepancy between data and image SNR highlights the potential impact of image reconstruction artifacts, such as clutter, which may degrade image quality despite relatively high-quality data.

The portable system demonstrated the lowest data SNR (7.9 ± 0.6 dB), reflecting the limitations imposed by its lower output power and dynamic range. However, the image SNR of the portable system (13 ± 3 dB) was comparable to the bench-top system, suggesting that while the raw data may be noisier, the portable system’s image reconstruction process was relatively effective at mitigating noise.

Image accuracy

The accuracy of the reconstructed images was evaluated by analyzing the intensity dependence on the target’s position within the

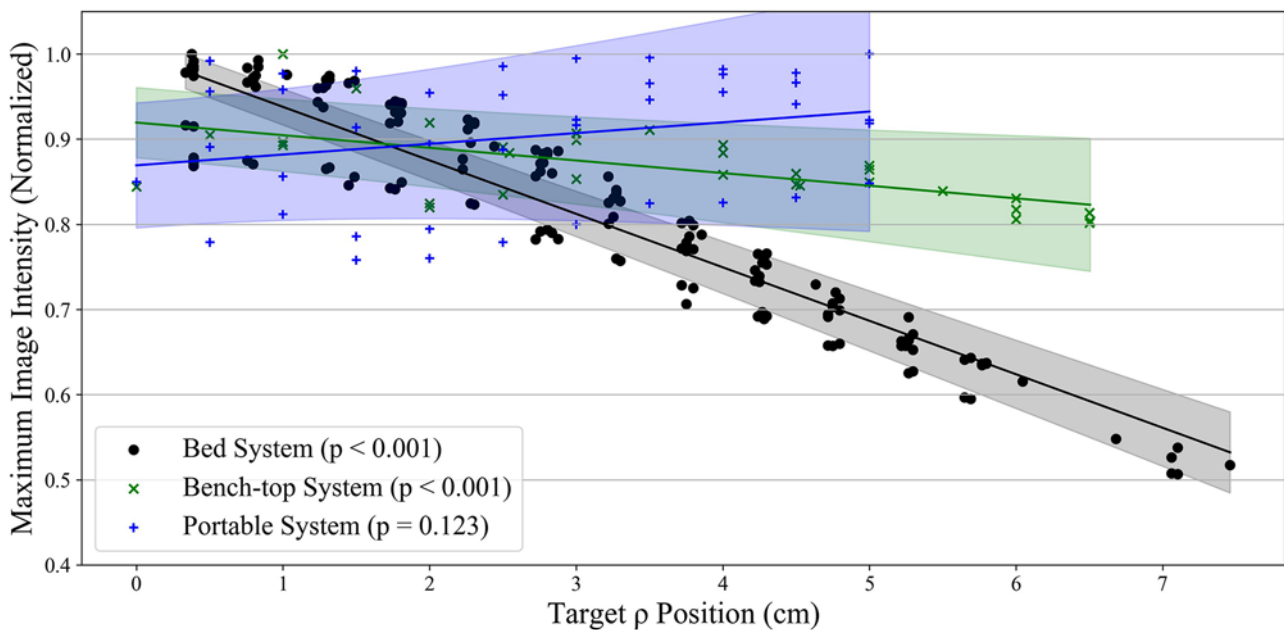


Figure 7. Maximum target image intensity versus target polar radius position for the three imaging systems. The linear fit and uncertainties are in the shaded regions. The *p*-values against the null hypothesis of zero slope are shown in parentheses in the legend.

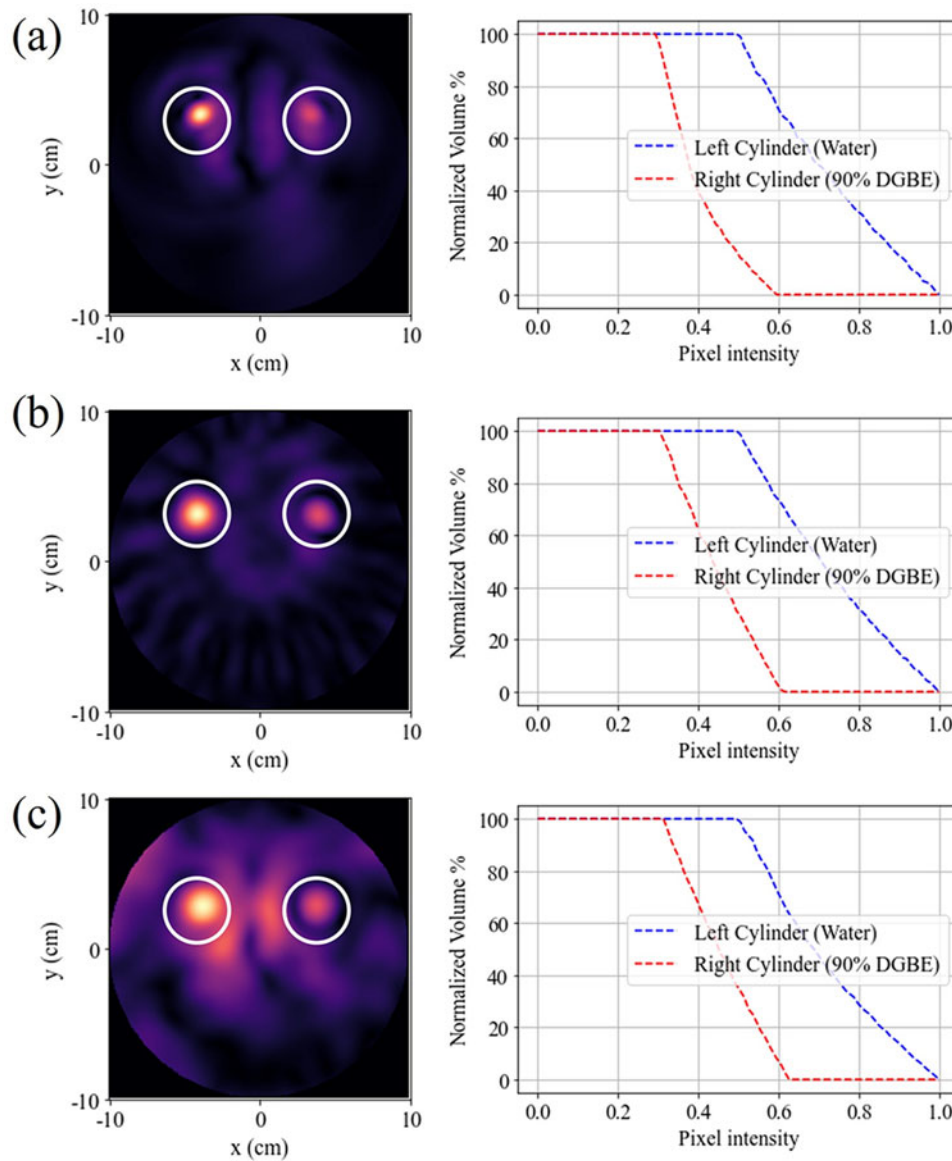


Figure 8. DAS-reconstructed images (left) and intensity-volume histograms (right) of water vs. 90% DGBE for the (a) bed system, (b) bench-top system, and (c) portable system.

imaging chamber (Fig. 7). In both the bed-based and bench-top systems, a noticeable intensity drop was observed as the target moved further from the centre. For the bed-based system, the target intensity decreased by a factor of two when the polar coordinate increased from 0 to 7 cm. The bench-top system exhibited a smaller drop, with the intensity reducing to 80% of its maximum value over the same distance.

In contrast, the portable system showed no clear intensity dependence on polar position. This may be due to the use of ultra-wideband (UWB) antennas, which produce a more uniform beam pattern, unlike the directional antennas used in the bed-based and bench-top systems.

Contrast

IVHs were constructed to determine the contrast between tumor-mimicking (water) and adipose-mimicking (90% DGBE) mate-

rials (Fig. 8), and tumor-mimicking (water) and fibroglandular-mimicking (50% DGBE) materials (Fig. 9).

The contrast $C_v^{\%}$ at a given percent volume was found for the three imaging systems (Fig. 10). For the tumor vs. fibroglandular scenario, the contrasts between each system were comparable. For the tumor vs. adipose scenario, the contrast was highest for the bed system and lowest for the portable system.

The contrast was found between the water and 11 solutions of varying-percent DGBE. The mean and standard deviation $C_v^{\%}$ was found for all three imaging systems (Fig. 11).

When the DGBE concentration in the secondary cylinder dropped below 40%, the contrast values $C_v^{\%}$ for all systems fell below 0.1, making it difficult to distinguish between the two targets. At the lowest concentration (10% DGBE), the bed-based system produced negative contrast values, suggesting that the lower reflectivity object appeared brighter than expected.

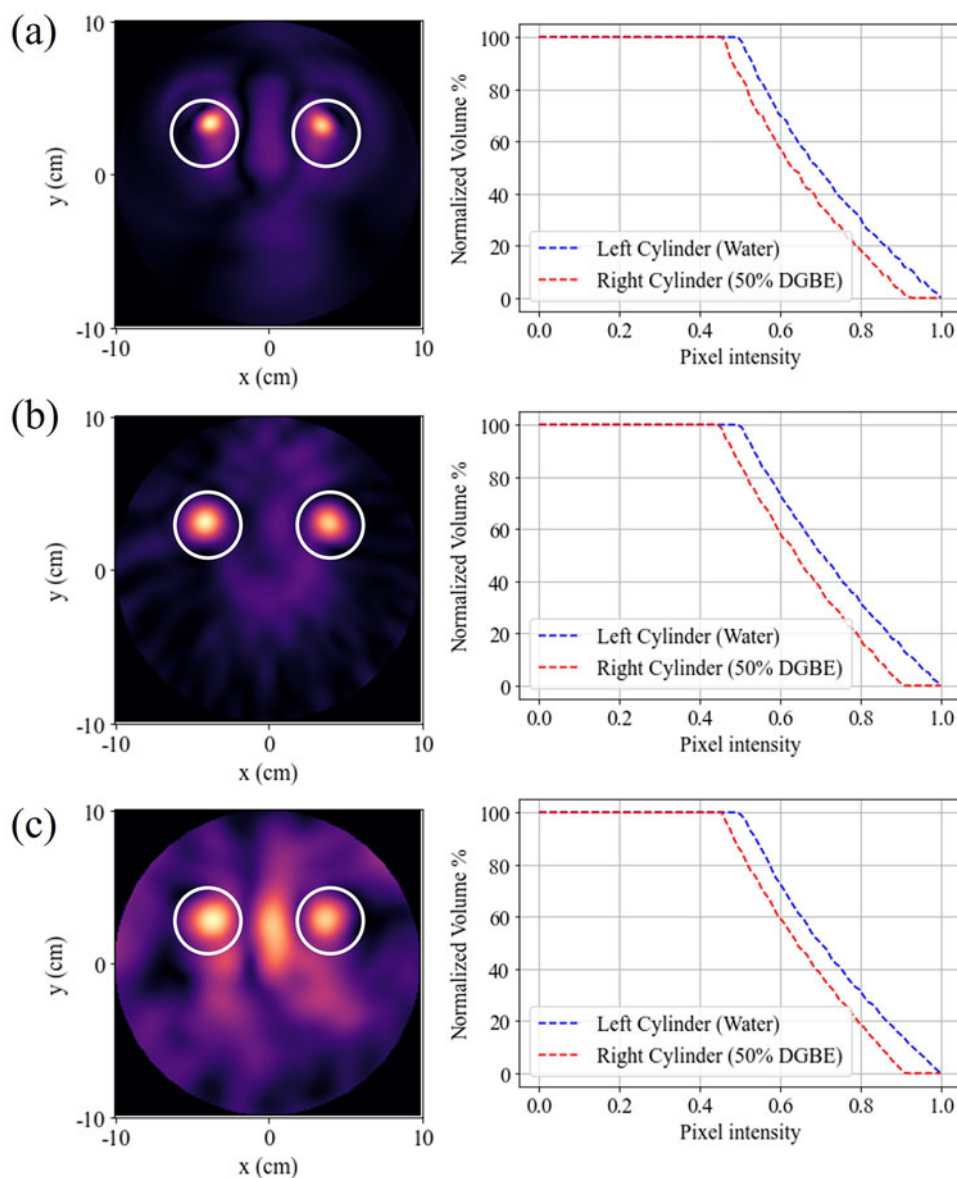


Figure 9. DAS-reconstructed images (left) and intensity-volume histograms (right) of water vs. 50% DGBE for the (a) bed system, (b) bench-top system, and (c) portable system.

Discussion

Three distinct methods were employed to assess the spatial resolution of the BMS systems. Among them, the modulation transfer function method yielded the highest spatial resolution, as it evaluates an idealized scenario where only a single-point source is present. However, while this method provides the best-case spatial resolution, it does not account for the presence of multiple scattering sources, which is a critical factor in clinical applications.

The two-target method offered a more realistic assessment of spatial resolution, as it incorporates the effects of scattering between two distinct targets. This makes it a more accurate representation of spatial resolution in complex environments, such as human breast tissue. Both the PSF and two-target methods depend heavily on the image reconstruction technique used. In this study, the delay-and-sum (DAS) beamformer was applied. However, more advanced reconstruction methods, such

as adaptive beamforming or machine-learning-based approaches, could further enhance the spatial resolution by improving the system's ability to mitigate scattering effects and refine image quality.

Conversely, the time-domain FWHM method provided the poorest resolution. This is likely because this method analyzes absolute-value time-domain data, which inherently overlooks constructive and destructive interference patterns introduced from various sampling angles. As a result, the data-based approach may fail to accurately capture fine spatial details, reinforcing the importance of selecting an appropriate reconstruction method tailored to the system's imaging environment.

Interestingly, the bed-based system achieved the best spatial resolution despite having a lower bandwidth compared to the bench-top system. This suggests that factors beyond bandwidth, such as antenna type, configuration, and system geometry, play

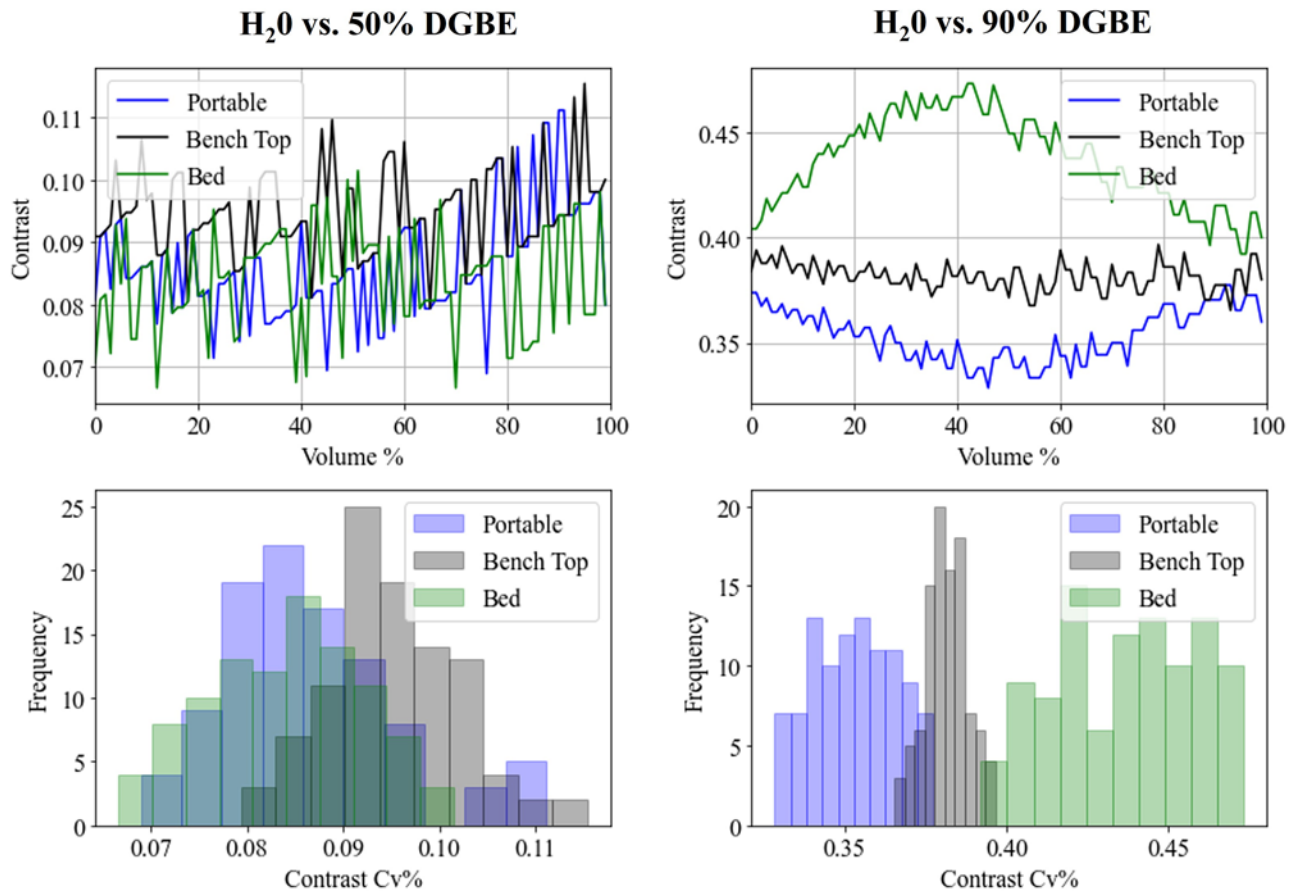


Figure 10. Contrast $C_v\%$ vs. percent-volume (top) and their corresponding histograms (bottom) for water vs. 50% DGBE (left) and water vs. 90% DGBE (right).

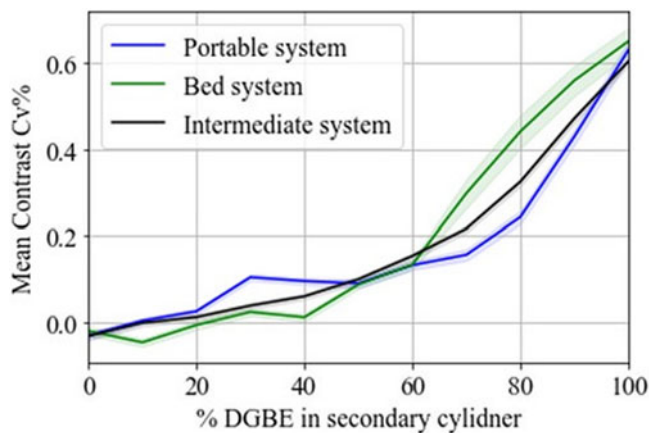


Figure 11. Mean contrast $C_v\%$ for the three imaging systems when varying the percent DGBE in the secondary cylinder. The standard deviation of the contrast $C_v\%$ is in the shaded region around the solid lines.

a role in determining spatial resolution. The bed-based system's optimized antenna configuration likely contributed to its superior performance, whereas the portable system exhibited the worst spatial resolution, which can be attributed to its limited bandwidth and lower-quality equipment. These findings indicate that while

bandwidth is important, other system design elements must be carefully considered to achieve optimal image quality.

The system noise was assessed by analyzing both the time-domain S_{11} signals and DAS-reconstructed images of repeated scans. The comparison between data and image noise metrics did not yield a clear consensus on which method produced a better signal-to-noise ratio (SNR), as performance varied across the systems.

The portable system, equipped with lower-power vector network analyzers (VNAs), showed higher levels of noise and clutter in its DAS images. The limited dynamic range and output power of the portable system's VNAs are likely responsible for these artifacts, as these factors directly influence the system's ability to detect weak signals. Despite these shortcomings, the image SNR of the portable system was comparable to that of the bench-top system, suggesting that other factors—such as clutter, artifacts, or reconstruction algorithms—may be more influential in determining overall image quality.

A notable difference was observed in the intensity dependence of the bed-based and bench-top systems with respect to the target's polar coordinates. This non-uniformity in intensity could impact the accuracy of spatial resolution measurements, especially in the two-target method, where one rod was fixed at the center and the other was moved outward. In this case, the intensity dependence may affect the perceived point at which the two targets become distinguishable.

Conversely, the portable system exhibited no clear intensity dependence on polar coordinates, likely due to the more uniform radiation pattern of its ultra-wideband (UWB) antennas. These antennas irradiate more uniformly in all directions compared to the more directional antennas used in the other systems. While this uniformity may have advantages, additional factors such as target size, symmetry, and shape should be explored in the future to gain a more comprehensive understanding of intensity behavior across different systems.

In terms of contrast resolution, the bed-based system outperformed the other systems, particularly in distinguishing between tumor-mimicking (water) and adipose-mimicking (90% DGBE) materials. However, as the dielectric contrast between the objects decreased, the performance of all systems converged. For example, when the concentration of DGBE in the secondary cylinder dropped below 40%, the contrast values $C_v^{\%}$ fell below 0.1, making it difficult to distinguish the objects. Notably, at a 10% DGBE concentration, the bed-based system produced negative contrast values, indicating that the lower reflectivity object appeared to have higher intensity—a phenomenon that may warrant further investigation.

The proposed method for contrast resolution analysis is the simplest approach, using two targets in the air. For future work, it would be beneficial to repeat these contrast resolution analyses with more realistic breast phantoms to determine the systems' true capabilities in a clinical setting.

Conclusion

A comprehensive image quality analysis was performed on three BMS systems to understand the effects of system design on image quality. A microwave-based bed system, bench-top system, and portable system were evaluated in terms of spatial resolution, noise, image accuracy, and contrast. The bench-top system, despite having the largest bandwidth of 7.3 GHz, was found to have worse spatial resolution than the bed system. The bed system achieved a minimum spatial resolution of 12.4 ± 5 mm when evaluating the PSF and MTF of a single target. The portable system had the lowest spatial resolution due to its small bandwidth of 3.8 GHz and equipment limitations. The bed-based system had the best SNR, followed by the bench-top system, and finally the portable system. The portable system had the least intensity dependence on polar positions within the imaging chamber, whereas the bed systems intensities varied as much as 50%. Each system was able to distinguish adipose-mimicking versus tumor-mimicking targets, with the bed-system producing the greatest contrast. The systems were able to distinguish fibroglandular and tumor targets; however, objects with closer dielectric properties will prove more difficult to differentiate. This work provides valuable assessment on image quality that can inform other microwave-based imaging systems, aiding in the advancement of system design and performance.

Acknowledgements. This research is funded by a Canadian Cancer Society Research Training Award – PhD in partnership with CancerCare Manitoba (CCS award #707895). The authors would like to acknowledge funding from the Natural Sciences and Engineering Research Council of Canada, the University

of Manitoba, the Canadian Cancer Society, and the CancerCare Manitoba Research Foundation.

Competing interests. The author(s) declare none.

References

- Coleman C (2017) Early detection and screening for breast cancer. *Seminars in Oncology Nursing* 33(2), 141–155.
- Wang L (2017) Early diagnosis of breast cancer. *Sensors* 17(7), 1572.
- Niell BL, Freer PE, Weinfurter RJ, Arleo EK and Drukteinis JS (2017) Screening for breast cancer. *Radiologic Clinics of North America* 55(6), 1145–1162.
- Aleshire ME, Adegboyega A, Escontrías OA, Edward J and Hatcher J (2021) Access to care as a barrier to mammography for black women. *Policy, Politics, & Nursing Practice* 22(1), 28–40.
- Wagh B, Chaluvayaswamy R and Pal D (2017) Assessment of adaptive breast cancer screening policies for improved mortality reduction in low to middle income countries. *Asian Pacific Journal of Cancer Prevention* 18(9), 2375–2380.
- da Costa Vieira RA, Biller G, Uemura G, Ruiz CA and Curado MP (2017) Breast cancer screening in developing countries. *Clinics (Sao Paulo, Brazil)* 72(2), 244–253.
- Modiri A, Goudreau S, Rahimi A and Kiasaleh K (2017) Review of breast screening: Towards clinical realization of microwave imaging. *Medical Physics* 44(12), 10.
- O'Loughlin D, O'Halloran M, Moloney BM, Glavin M, Jones E and Elahi MA (2018) Microwave breast imaging: Clinical advances and remaining challenges. *IEEE Transactions on Biomedical Engineering* 65(11), 2580–2590.
- Wang L (2023) Microwave imaging and sensing techniques for breast cancer detection. *Micromachines* 14(7), 1462.
- AlSawafah N, El-Abed S, Dhou S and Zakaria A (2022) Microwave imaging for early breast cancer detection: Current state, challenges, and future directions. *Journal of Imaging* 8(5), 123.
- Reimer T and Pistorius S (2023) Review and analysis of tumour detection and image quality analysis in experimental breast microwave sensing. *Sensors (Basel, Switzerland)* 23(11), 5123.
- Porter E and O'Loughlin D (2022) Pathway to demonstrating clinical efficacy of microwave breast imaging: Qualitative and quantitative performance assessment. *IEEE Journal of Electromagnetics, RF and Microwaves in Medicine and Biology* 6(4), 439–448.
- Reimer T, Eashour F, Fontaine G, Krenkevich J and Pistorius S (2024) Evaluating system design in breast microwave sensing: Data and image quality in multiple systems. In *2024 18th European Conference on Antennas and Propagation (EuCAP)*, pp. 1–5.
- Solis-Nepote M, Reimer T and Pistorius S (2019) An air-operated bistatic system for breast microwave radar imaging: Pre-clinical validation. In *Annual International Conference of the IEEE Engineering in Medicine and Biology Society*, pp. 1859–1862.
- Fontaine G, Jelani A and Pistorius S (2024) Calibration stability and localization accuracy of a low-cost and portable breast microwave sensing device. Montreal, QC, Canada: IEEE Xplore. In *2024 IEEE MTT-S International Microwave Biomedical Conference (IMBioC)*, pp. 48–50.
- Reimer T, Solis-Nepote M and Pistorius S (2019) The impact of the inverse chirp z-transform on breast microwave radar image reconstruction. In *2019 European Microwave Conference in Central Europe (EuMCE)*, pp. 626–629.
- Reimer T and Pistorius S (2023). A methodology for evaluating image resolution in experimental breast microwave imaging Florence, Italy IEEE Xplore. In *2023 17th European Conference on Antennas and Propagation (EuCAP)*, pp. 1–5.



Tyson Reimer is a Ph.D. student in Medical Physics at the University of Manitoba. He holds a B.Sc. (Hons.) in Medical & Biological Physics and M.Sc. in Medical Physics, both from the University of Manitoba. His research interests include image reconstruction and image quality analysis in microwave-based breast imaging.



Jordan Krenkevich is currently a Software Quality Assurance Analyst at Circle Cardiovascular Imaging, Calgary, Alberta, Canada. He received the B.Sc. in Biological and Medical Physics (hons) at the University of Manitoba, Winnipeg, Canada, in 2021. Currently an M.Sc. student at the University of Manitoba, his research focuses on improving testing methods for pre-clinical breast microwave sensing systems.



Gabrielle Fontaine received the B.Sc. in Medical Physics and Biological Sciences (hons) at the University of Manitoba, Winnipeg, Canada in 2020, and the M.Sc. in physics at the University of Manitoba, Winnipeg, Canada in 2022. Currently a Ph.D. student, her research focuses on developing and testing a portable microwave system for early breast cancer detection.



Stephen Pistorius is the Associate Head: Medical Physics and Professor in Physics and Astronomy, Radiology and Biomedical Engineering at the University of Manitoba. He is a Senior Scientist at the CancerCare Manitoba Research Institute, a Fellow of the Canadian Organization of Medical Physicists and a Professional Physicist (P.Phys.). He holds an Hons. B.Sc. (radiation physics), M.Sc. (medical science), and Ph.D. (physics) from the University of Stellenbosch, South Africa, and a Post-Graduate Diploma in Business Management from the Edinburgh Business School, UK. His research interests focus on image processing and reconstruction, medical device development, and understanding radiation transport in clinically useful imaging and treatment modalities.



Fatimah Eashour received her M.Sc. in physics at the University of Manitoba, Winnipeg, Canada. She is a Ph.D. candidate in Medical Physics at the University of Manitoba.